Structures of flow with particles saltating over the permeable fixed rough bed

Yuya Takakuwa
Civil, Human and Environmental Engineering, Chuo University
1-13-27 Kasuga, Bunkyo-ku, Tokyo, Japan 112-8551
Tel. +81 (03) 3817 1615, Email: a18.ntwb@g.chuo-u.ac.jp

Shoji Fukuoka
Research and Development Initiative, Chuo University
Email: sfuku@tamacc.chuo-u.ac.jp

In this paper, first, the applicability of the numerical method (APM [2,3]) using the one-fluid model of solid-liquid multiphase based on the Cartesian coordinate system is examined to the experiment of turbulent flow over the permeable fixed rough bed. It is shown that vertical profiles of streamwise velocity and turbulence intensity follow the results of Manes' experiment only if the volume fraction of solid phase is estimated with high accuracy, even if cell sizes are not small. Second, a three-dimensional numerical experiment is conducted about turbulent flow including particles saltating over the permeable fixed rough bed. Then, effects of saltating particles on the main flow are analyzed. With saltation of particle, the slow velocity of the low position is transported to the higher position, and the streamwise velocity of the high position is considerably becomes small. Therefore, the saltation of particle has an influence such as the turbulence ejection to the main flow. In this condition, turbulence intensities of the flow including moving particles become larger than those of the clear flow.

Key Words: *turbulent structures, effects of moving particles, the one-fluid model of solid-liquid multiphase, permeable fixed rough bed, Euler-Lagrange simulation*

1. Introduction

Gravel bed rivers are composed of large particles as gravels and cobbles, and particles of various sizes move on the gravel bed. Therefore, it is important to clarify the mechanism of interaction between the flow and moving particles in the vicinity of the gravel bed. Structures of flow with the moving particles change compared with those without particles, in addition, measurements of flow around moving particles are difficult even in laboratory flumes.

In the calculation of flow with solid particles, it is not easy to set up fluid calculation cells adapting to the moving boundary in every step. In recent years, the Euler-Lagrange solvers (MICS [1] and APM [2, 3]) using the one-fluid model of solid-liquid multiphase were proposed to fluid calculation cells including solid phase in the Cartesian coordinate system. Then, interactions between flow and particles are considered dynamically.

In this paper, first, 3D numerical experiments are conducted by APM about turbulent flow over the permeable fixed rough bed. The results of the numerical experiments are compared with those of laboratory experiment (Manes et al. [4]), and applicability and accuracy of the APM are confirmed. Second, the 3D numerical experiment is performed about turbulent flow including moving particles over the permeable fixed rough bed, and changes in the flow structures due to the moving particles are examined.

2. Numerical method

The basic equations of fluid motion are described as follows:

$$\frac{\partial u_i}{\partial x_i} = 0 \tag{1}$$

$$\frac{Du_i}{Dt} = g_i - \frac{1}{\rho}\frac{\partial P}{\partial x_i} + \frac{\partial}{\partial x_j}\{2(\nu + \nu_t)S_{ij}\} \tag{2}$$

$$S_{ij} = \frac{1}{2}\left(\frac{\partial u_i}{\partial x_j} + \frac{\partial u_j}{\partial x_i}\right) \tag{3}$$

$$\nu_t = (C_s\Delta)^2\sqrt{2S_{ij}S_{ij}} \tag{4}$$

where u_i: ith component of mass averaged velocity, P: sum of the pressure and isotropic component of SGS stress, g_i: ith component of gravitational acceleration, ρ: volume averaged density, ν: kinematic viscosity, ν_t:SGS turbulent viscosity,

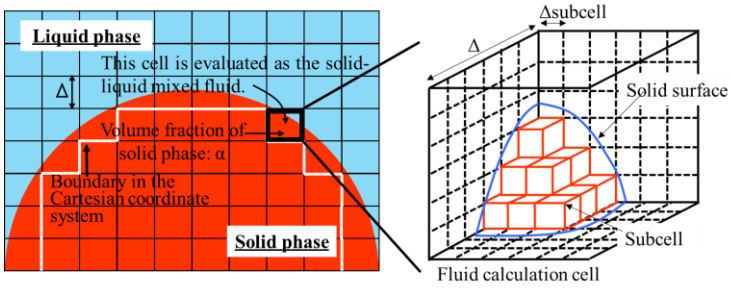

(a) (b)

Fig. 1. (a) Methodology of fluid calculation for cells containing solid phase using the one-fluid model of solid-liquid multiphase, and (b) concept of the subcell method to evaluate the volume fraction of solid phase.

S_{ij}: strain rate tensor, C_s: Smagorinsky constant and Δ: computational cell size.

Fig. 1 (a). shows the methodology of the one-fluid model of solid-liquid multiphase for cells containing solid phase, and the cells are dealt as solid-liquid mixed fluid. Mass and momentum of mixed fluid are evaluated using the volume fraction of solid phase "α" (see Eq. (5-6)), and fluid motions are calculated.

$$\rho = \alpha\rho_s + (1-\alpha)\rho_f \tag{5}$$

$$\rho u_i = \alpha\rho_s u_{s,i} + (1-\alpha)\rho_f u_{f,i} \tag{6}$$

where suffixes *s* and *f* denote solid phase and liquid phase, respectively. The volume fraction of solid phase influences evaluation of the velocity of mixed fluid directly, and its precision has large influence on the velocity distribution in the vicinity of boundaries. The volume fraction of solid phase is evaluated by the subcell method (see **Fig. 1 (b).**).

Particle motions are calculated by the momentum equations and the angular momentum equations of rigid bodies:

$$M\ddot{\boldsymbol{r}}_{\boldsymbol{G}} = M\boldsymbol{g} + \boldsymbol{F_f} + \boldsymbol{F_c} \tag{7}$$

$$\dot{\boldsymbol{\omega}}_{\boldsymbol{r}} = \boldsymbol{I}_{\boldsymbol{r}}^{-1}\left\{\boldsymbol{R}^{-1}\left(\boldsymbol{N_f} + \boldsymbol{N_c}\right) - \boldsymbol{\omega}_{\boldsymbol{r}} \times \boldsymbol{I}_{\boldsymbol{r}}\boldsymbol{\omega}_{\boldsymbol{r}}\right\} \tag{8}$$

where the bold face letters indicate vector tensor and matrix, *M*: mass of particle, $\boldsymbol{r_G}$: position of center of gravity, $\boldsymbol{g}$: gravitational acceleration, $\boldsymbol{F}$: forces on particle surfaces, $\boldsymbol{N}$: torque on particles, $\boldsymbol{\omega}$: angular velocity, $\boldsymbol{R}$: transformation matrix (from the local coordinate system to the global coordinate system), and $\boldsymbol{I}$: tensor of momentum inertia. Suffixes *f* and *c* denote fluid force and contact force, respectively, and suffix *r* denotes components in local coordinate systems of each particle.

3. Applicability and accuracy of APM for the turbulent flow over permeable fixed rough bed

Fig. 2. shows the methodology and measurement lines of the 3D numerical experiments reproducing the laboratory experiment of Manes et al. [4]. The channel was 24d long, 10d width and 5 layers spheres of d=12[mm] were placed regularly at the bed. Bed slope was i_b=1/400 as same as Manes et al., and periodic boundary conditions were applied in the streamwise and spanwise directions. The flow depth from the roughness top (Z=0) to free surface was h=42[mm] which gave a relative submergence ratio of h/d=3.5. Densities of liquid phase and solid phase were $\rho_f = 1000$ and $\rho_p = 2500\ [kg/m^3]$, respectively. **Tab. 1.** shows the calculation conditions of numerical experiments. The experiments of 6 cases were conducted [5] with different cell sizes Δ (d/Δ=5, 10 and 20) and subcell sizes $\Delta_{subcell}$ ($\Delta/\Delta_{subcell}$=2 and 6). In this paper, case 2, 4, 5 and 6 are shown. Time steps for fluid calculation (dt_f) were set so that the the Courant number were 0.1, and those for sampling of turbulent flow were dt_f=1.00×10^{-3}[s].

Fig. 3 (a). shows time and space averaged velocities of numerical and laboratory experiments. But, the velocities in z/d>2 were not measured in the laboratory experiment [4]. In case 6 which were set fluid calculation cells and subcells smallest, respectively, the velocity distribution reproduced in neighborhood of top of permeable layer, although it was slightly bigger than the result of laboratory experiment. In addition, in case 4 which were set subcells small ($\Delta/\Delta_{subcell}$=6), and calculation fluid cells not small (d/Δ=10), the velocity distribution almost followed the result of laboratory experiment. Then, turbulence intensities were compared (see **Fig. 3 (b)**). In case 4, peak values of streamwise and vertical components of turbulence intensity and heights taking the peak value almost reproduced.

From the above results, it was confirmed that flow structures over permeable fixed rough bed were explained by APM only if the volume fraction of solid phase "α" was estimated with high accuracy ($\Delta/\Delta_{subcell}$=6), even if cell sizes were not small (d/Δ=10).

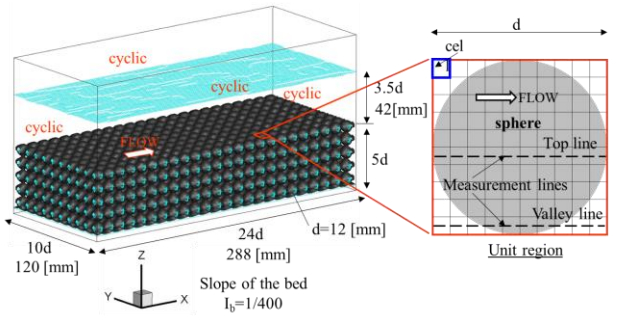

(a) (b)

Fig. 2. (a) Computational domain and boundary conditions, and (b) measurement lines.

Tab. 1. Conditions of numerical experiments.

	case2	case4	case5	case6
cell size Δ[mm]	2.4	1.2	0.6	0.6
d/Δ	5	10	20	20
subcell size $\Delta_{subcell}$[mm]	0.4	0.2	0.3	0.1
$\Delta/\Delta_{subcell}$	6	6	2	6
dt_f[s]	5.00×10^{-4}	2.50×10^{-4}	1.25×10^{-4}	1.25×10^{-4}
dt_t[s]	1.00×10^{-3}	1.00×10^{-3}	1.00×10^{-3}	1.00×10^{-3}

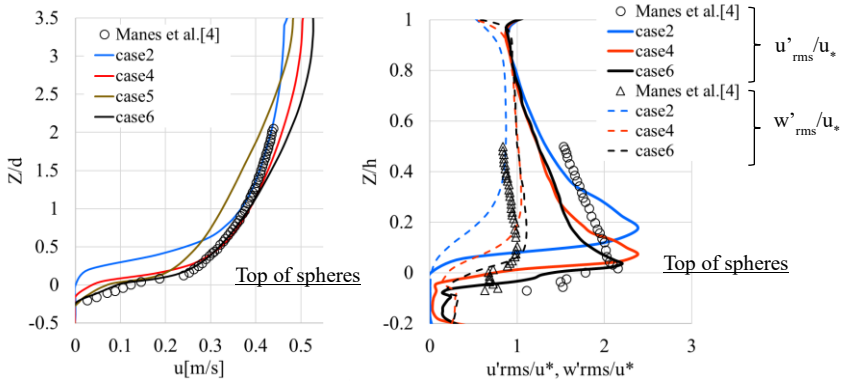

(a) (b)

Fig. 3. The comparison of numerical results (curve) and experimental results [4] (symbol) of (a) Streamwise velocity, (b) Root-mean-square of velocity fluctuations (u'_{rms}/u_*: solid curves, and w'_{rms}/u_*: dashed curves). The friction velocity was 0.0308[m/s].

4. Changes in flow structures with moving large particles

The 3D numerical experiment was performed in a 240d long, 20d width and 1/50 bed slope with the same structures of permeable layer as the numerical experiments of **3**. Steady flow Q_f=12.8[L/s] was given. Velocity distributions of the upper boundary condition were given to the reference section (X=0.47[m]) in every step to make the boundary layer develop in the short distance. But, for the stability of the calculation, spanwise component of velocity was zero. Periodic boundary condition was adapted in the spanwise direction. The flow depth of the clear flow was h=42[mm] from the roughness top (Z=0) to free surface. Spheres of d=12[mm] were thrown in the region of 0.6≤X≤1.0 [m] and Z=0.05[m] at random (particle concentration: c=0.5%). Initial velocities of particle were u=1.2[m/s] to follow flow. Time step for fluid calculation $dt_f=5.00\times10^{-5}$[s], and that for sampling of turbulent flow $dt_t=4.00\times10^{-4}$[s]. In addition, densities of fluid and particles ρ_f=1000 and ρ_p=2500 [kg/m^3], coefficient of restitution e=0.7, elastic modulus $E=8.0\times10^{10}$[Pa], Poisson's ratio 0.23, coefficient of friction 0.2, and time step for particle motion $dt_p=2.50\times10^{-7}$[s].

In this paper, the particle-A was focused (**Fig. 4.**), and changes in flow structures with saltating large particles were examined. Fluid around the saltating particle-A moved with it. Therefore, the upward velocity occurred in the upper side of the particle-A (**Fig. 4 (c)**), and the slow water mass at the low position was transported to higher position (**Fig. 4 (b)**). **Fig. 5.** shows time series of three components of velocity at the point P1 (see **Fig. 4 (b)** and **(c)**). Upward velocities occurred momentarily at the P1 in the times (about 13.4 and 13.7[s]) when particles jumped at the position lower than P1, and then the streamwise velocities considerably became small. So, this means that saltations of large particles behave as the turbulence ejection to the main flow.

Finally, time and space averaged flow structures were examined (see **Fig. 6.**). The velocity distribution of flow including particles became small slightly in comparison with that of the clear flow. In this case, effects of moving large particles on averaged streamwise velocity were small because the particle concentration was small. On the other hand, the turbulence intensities became larger than those of the clear flow in Z>0.5d, and this result was different from the result of the numerical experiment (Chan-Braun et al. [6]). Because, in our numerical experiment, specific gravity was 2.5, and therefore saltating large particles more disturbed main flow than case of Chan-Braun et al. using the particles of specific gravity 1.7.

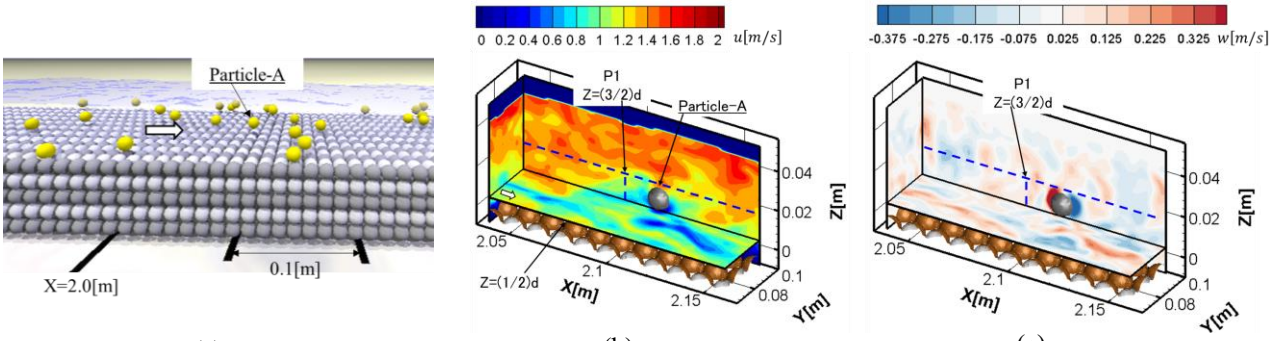

(a) (b) (c)

Fig. 4. Snapshots of the simulation result, (a) Motions of particles, (b) and (c) Contours of streamwise and vertical velocities around particle-A.

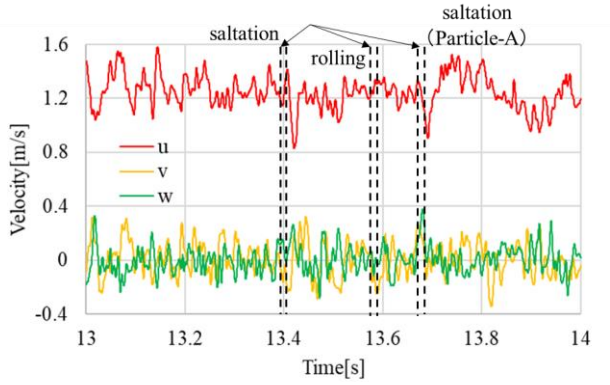

Fig. 5. Time series of velocity fluctuation at the point-P1 (see Fig. 4). In the times enclosed by dashed lines (about 13.4, 13.6 and 13.7[s]), some particles passed a bottom from the point P1.

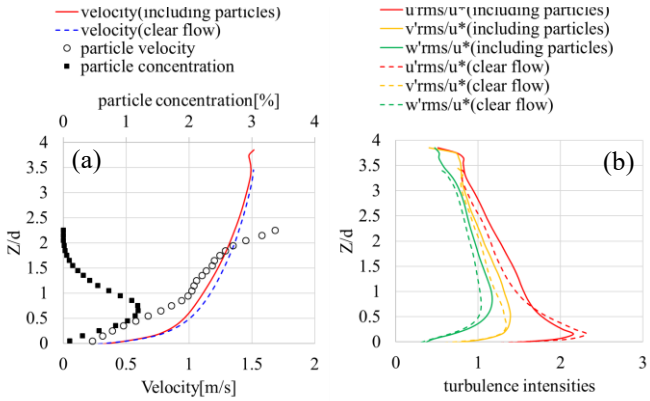

Fig. 6. The comparison of results of the flow including particles (solid curve) and those of clear flow (dashed curve) of (a) Time and space averaged streamwise velocity, (b) Time and space averaged turbulence intensities. The friction velocity of the flow including particles was 0.095[m/s], and that of clear flow was 0.091[m/s]. Streamwise velocity and concentration of particles are plotted in (a).

5. Conclusion

It was confirmed that flow structures over the permeable fixed rough bed were explained by APM only if the volume fraction of solid phase was estimated with high accuracy ($\Delta/\Delta_{subcell}$=6), even if cell sizes were not small (d/Δ=10).

Second, the 3D numerical experiments was conducted about turbulent flow including particles moving over permeable fixed rough bed. It was shown that saltations of large particle behave as the turbulence ejection to the main flow. Moreover, in this condition, turbulence intensities of the flow including moving particles became larger than those of the clear flow.

Numerical experiments of higher particle concentrations are in progress and to be presented in the Conference.

References

[1] Ushijima, S., Yamada, S., Fujioka, S. and Nezu, I.: Prediction method (3D MICS) for transportation of solid bodies in 3d free-surface flows, *JSCE B Vol.62(1), pp.100-110*, 2006 (*in Japanese*).

[2] Fukuoka, S., Fukuda, T. and Uchida, T.: Effects of sizes and shapes of gravel particles on sediment transports and bed variations in numerical movable-bed channel, *Advances in Water Resources, Vol.72, pp.84-96*, 2014.

[3] Fukuda, T. and Fukuoka, S.: Interface-resolved large eddy simulations of hyperconcentrated flows using spheres and gravel particles, *Advances in Water Resources, https://doi.org/10.1016/j.advwatres.2017.10.037*, 2017.

[4] Manes, C., Pokrajac, D., McEwan, I. and Nikora, V.: Turbulence structure of open channel flows over permeable and impermeable beds: A comparative study, *Physics of Fluids, Vol.21, 125109*, 2009.

[5] Takakuwa, Y. and Fukuoka, S.: Application of the one-fluid model of solid-liquid multiphase to turbulent flow with a permeable rough boundary, *Proceeding of 32th CFD Symposium, E11-2*, 2018 (*in Japanese*).

[6] Chan-Braun, C., Garcia-Villalba, M. and Uhlman, M.: Direct numerical simulation of sediment transport in turbulent open channel flow, High Performance Computing in Science and Engineering'10, pp.295-306, 2011.